Commun. Korean Math. Soc. **22** (2007), No. 3, pp. 453–464

THREE-DIMENSIONAL NUMERICAL SIMULATIONS OF A PHASE-FIELD MODEL FOR ANISOTROPIC INTERFACIAL ENERGY

JUNSEOK KIM

ABSTRACT. A computationally efficient numerical scheme is presented for the phase-field model of two-phase systems for anisotropic interfacial energy. The scheme is solved by using a nonlinear multigrid method. When the coefficient for the anisotropic interfacial energy is sufficiently high, the interface of the system shows corners or missing crystallographic orientations. Numerical simulations with high and low anisotropic coefficients show excellent agreement with exact equilibrium shapes. We also present spinodal decomposition, which shows the robustness of the proposed scheme.

1. Introduction

In this paper, an efficient and accurate numerical scheme and its nonlinear multigrid solver are presented for solving the phase-field model with anisotropy interfacial energy. Phase-field models provide a useful numerical approach to study a wide variety of phase transformation processes [14, 15] because explicit tracking of the interface is not needed.

The fundamental idea of a phase-field model is to include an additional variable, or order parameter c, that denotes the phases in a multiphase system. The order parameter is constant in each bulk phase, e.g. $c = -1$ in the matrix phase and $c = 1$ in the particle phase. The interface between phases is represented by a smooth transition region where c varies from -1 to 1. The interfacial energy is accounted for by the addition of gradient energy terms that are nonzero in this transition region [3].

Strongly anisotropic surface energy is common in many semiconductor systems. In this case, the equilibrium shape of a crystal of the film material will have corners and edges where certain high energy orientations have been excluded. It is shown that the surface energy anisotropy, which may be modified

Received July 6, 2006; Revised July 2, 2007.

2000 *Mathematics Subject Classification.* 65M06, 65M55, 74N20.

Key words and phrases. phase-field model, anisotropy, interfacial energy, Cahn-Hilliard equation, nonlinear multigrid method.

This work was supported by the Korea Research Foundation Grant funded by the Korean Government(MOEHRD) (KRF-2006-C00225).

by the change in material composition and temperature, plays an important role in the island shape transition, self-organization, and stability of epitaxial islands [17]. There is an excellent work about the anisotropy with regularization [3], but it is restricted to two-dimensional computation only. Also, it is not an easy task to extend it to three-dimensional calculation with straightforward manner. But most physical problems which interest us require a three-dimensional calculation. Our goal in this paper is to present an efficient and accurate three-dimensional numerical scheme and solver.

The paper is organized as follows. In Section 2 we provide a brief description of the phase-field model for the system with anisotropy interface energy. Section 3 describes the numerical scheme and its nonlinear multigrid solver. Section 4 shows numerical results. Finally, conclusions are drawn in Section 5.

2. Phase-field model

We briefly review the phase field model for anisotropic interface energy. Phase-field models are natural extensions of the diffuse-interface models of Cahn and Hilliard [2]. The phase-field equations are developed from the free-energy functional,

$$\mathcal{F} = \int_{\Omega} \left(F(c) + \frac{\epsilon^2}{2} |\nabla c|^2 \right) d\Omega, \tag{1}$$

where Ω is the region occupied by the system. A free-energy density function, $F(c) = 0.25(1-c^2)^2$, is a double-well that has two minima at $c = -1$ and $c = 1$. Requiring the free-energy functional to decrease monotonically in time for a conserved order parameter results in the Cahn-Hilliard evolution equation

$$\frac{\partial c}{\partial t} = M \Delta \mu, \tag{2}$$

$$\begin{aligned} \mu = {} & f(c) - \nabla \cdot [\epsilon(\mathbf{n})^2 \nabla c] - \partial_x [|\nabla c|^2 \epsilon(\mathbf{n}) \partial_{c_x} \epsilon(\mathbf{n})] \\ & - \partial_y [|\nabla c|^2 \epsilon(\mathbf{n}) \partial_{c_y} \epsilon(\mathbf{n})] - \partial_z [|\nabla c|^2 \epsilon(\mathbf{n}) \partial_{c_z} \epsilon(\mathbf{n})], \end{aligned} \tag{3}$$

where M is the mobility. For simplicity, we consider a constant one ($M \equiv 1$). $f(c) = \partial_c F$ and ∂_ϕ are partial derivatives with respect to the variable ϕ. Anisotropy is included in this model by writing ϵ as a function of the local unit normal vector $\mathbf{n} = \nabla c / |\nabla c|$ in the interfacial region. Thus,

$$\epsilon(\mathbf{n}) = \epsilon_0 (1 - 3\epsilon_4) \left[1 + \frac{4\epsilon_4}{1 - 3\epsilon_4} \frac{c_x^4 + c_y^4 + c_z^4}{|\nabla c|^4} \right].$$

The constant parameters ϵ_0 and ϵ_4 are related to the strength and the magnitude of the anisotropy in the interface energy, respectively. The subscripts denote partial differentiation with respect to x, y, and z.

3. Numerical method for the phase field model

We employ a finite difference scheme to solve the phase field Eqs. (2) and (3). Semi-implicit time and centered difference space discretizations are used. The resulting discrete equations are solved using an efficient and accurate nonlinear multigrid method. For simplicity of presentation, we introduce two-dimensional numerical solution and three-dimensional one is a straightforward extension.

3.1. Discretization of the governing equations

In this section, we present fully discrete schemes for the equation. Let N_x and N_y be positive even integers, h be the uniform mesh size, and $\Omega_h = \{(x_i, y_j) : x_i = (i-0.5)h, y_j = (j-0.5)h,\ 1 \le i \le N_x,\ 1 \le j \le N_y\}$ be the set of cell-centers. Let c_{ij}^n denote the discretized phase field approximation of $c(x_i, y_j, t^n)$. Let us rewrite the Eq. (3) as

$$\mu = \nu + c^3 - 3c + s, \tag{4}$$

where $\nu = 2c - \epsilon_0^2 \Delta c$ and

$$\begin{aligned} s &= -\nabla \cdot [(\epsilon(\mathbf{n})^2 - \epsilon_0^2)\nabla c] - \partial_x[|\nabla c|^2 \epsilon(\mathbf{n}) \partial_{c_x} \epsilon(\mathbf{n})] \\ &\quad -\partial_y[|\nabla c|^2 \epsilon(\mathbf{n}) \partial_{c_y} \epsilon(\mathbf{n})]. \end{aligned} \tag{5}$$

We lag s in the Eq. (4) and discretize the Eqs. (2) and (4) by using a semi-implicit scheme in time and a centered difference one in space. Thus, we write the discrete equations as follows:

$$\frac{c_{ij}^{n+1} - c_{ij}^n}{\Delta t} = \Delta_d \nu_{ij}^{n+1} + \Delta_d[(c_{ij}^n)^3 - 3c_{ij}^n + s_{ij}^n], \tag{6}$$

$$\nu_{ij}^{n+1} = 2c_{ij}^{n+1} - \epsilon_0^2 \Delta_d c_{ij}^{n+1}, \tag{7}$$

where Δ_d denotes the standard five point difference approximation of Δ. That is, $\Delta_d c_{ij} = (c_{i-1,j} + c_{i+1,j} - 4c_{ij} + c_{i,j-1} + c_{i,j+1})/h^2$. The first term in s, $\nabla \cdot [(\epsilon(\mathbf{n})^2 - \epsilon_0^2)\nabla c]$, is discretized as follows.

$$\begin{aligned} &(\nabla \cdot [(\epsilon(\mathbf{n})^2 - \epsilon_0^2)\nabla c])_{ij} \\ = \ &[(\epsilon(\mathbf{n})^2 - \epsilon_0^2)_{i+\frac{1}{2},j}(c_{i+1,j} - c_{ij}) \\ &-(\epsilon(\mathbf{n})^2 - \epsilon_0^2)_{i-\frac{1}{2},j}(c_{ij} - c_{i-1,j}) + (\epsilon(\mathbf{n})^2 - \epsilon_0^2)_{i,j+\frac{1}{2}}(c_{i,j+1} - c_{ij}) \\ &-(\epsilon(\mathbf{n})^2 - \epsilon_0^2)_{i,j-\frac{1}{2}}(c_{ij} - c_{i,j-1})]/h^2. \end{aligned}$$

For the second term, $\partial_x[|\nabla c|^2 \epsilon(\mathbf{n}) \partial_{c_x} \epsilon(\mathbf{n})]$, first analytically calculate the term inside bracket and then apply a central difference approximation. The third one is treated with similar manners. One of the important features of this scheme is that we can take a large time step by the convexity splitting type temporal discretization [4, 9]. Another feature is that we incorporate fast solvers, nonlinear multigrid methods for the Cahn-Hilliard equations [7], into the resulting scheme.

3.2. Stability of the proposed scheme

In this section, we will discuss the stability of the scheme, Eqs. (6) and (7). Several other schemes for phase-field models (Eqs. (2) and (3)) with anisotropic interfacial energy have been developed by many authors. For example, in [3], a regularization in the numerical scheme was employed to enforce local equilibrium at the corners. In [12], an explicit scheme was used and the time step, Δt, is proportional to h^4. This time step restriction becomes very severe when the space step, h, is small. In the isotropic case (ϵ is constant in the free-energy functional, Eq.(1)), we have $s_{ij}^n \equiv 0$ in the Eq. (6) and recover an unconditionally gradient stable scheme as in [4]. For the anisotropic case, since we subtract the dominant part, $\nabla \cdot (\epsilon_0^2 \nabla c)$, in Eq. (5), s is a source with a small deviation. Therefore, we inherit a good stability property from the isotropic case and this property is validated by numerical experiments.

3.3. A nonlinear multigrid method

In this section, we develop a nonlinear Full Approximation Storage (FAS) multigrid method to solve the nonlinear discrete system (6) and (7) at the implicit time level. See the reference text [13] and the paper [8] for additional details and background. The algorithm of the nonlinear multigrid method for solving the discretized system is given as follows: First, let us rewrite Eqs. (6) and (7) in the form of

$$\begin{aligned} N(c^{n+1}, \nu^{n+1}) &= (\phi^n, \psi^n), \\ \text{where } N(c^{n+1}, \nu^{n+1}) &= \left(\frac{c_{ij}^{n+1}}{\Delta t} - \Delta_d \nu_{ij}^{n+1},\ \nu_{ij}^{n+1} - 2c_{ij}^{n+1} + \epsilon_0^2 \Delta_d c_{ij}^{n+1} \right), \\ (\phi^n,\ \psi^n) &= \left(\frac{c_{ij}^n}{\Delta t} + \Delta_d[(c_{ij}^n)^3 - 3c_{ij}^n + s_{ij}^n],\ 0 \right). \end{aligned}$$

Given the number β of pre- and post-smoothing relaxation sweeps, an iteration step for the nonlinear multigrid method using the V-cycle is formally written as follows [13]:

FAS multigrid cycle

$$\{c_k^{m+1}, \nu_k^{m+1}\} = FAScycle(k, c_k^m, \nu_k^m, N_k, \phi_k^n, \psi_k^n, \beta).$$

Now, define the FAScycle.

step 1) *Presmoothing*

$$\{\bar{c}_k^m,\ \bar{\nu}_k^m\} = SMOOTH^{\beta}(c_k^m, \nu_k^m, N_k, \phi_k^n, \psi_k^n),$$

which means performing β smoothing steps with the initial approximations c_k^m, ν_k^m, source terms ϕ_k^n, ψ_k^n, and $SMOOTH$ relaxation operator to get the approximations $\bar{c}_k^m$, $\bar{\nu}_k^m$. One $SMOOTH$ relaxation operator step consists of solving the system (8) and (9) given below by 2×2 matrix inversion for each

i and j. Rewriting Eqs. (6) and (7), we get

$$\begin{aligned}\frac{c_{ij}^{n+1}}{\Delta t}+\frac{4\nu_{ij}^{n+1}}{h^2} &= \phi_{ij}^n+\frac{\nu_{i+1,j}^{n+1}+\nu_{i-1,j}^{n+1}+\nu_{i,j+1}^{n+1}+\nu_{i,j-1}^{n+1}}{h^2},\\ \frac{h^2+2\epsilon_0^2}{(h^2/2)}c_{ij}^{n+1}-\nu_{ij}^{n+1} &= -\psi_{ij}^n+\frac{c_{i+1,j}^{n+1}+c_{i-1,j}^{n+1}+c_{i,j+1}^{n+1}+c_{i,j-1}^{n+1}}{(h^2/\epsilon_0^2)}.\end{aligned}$$

Now, we replace c_{kl}^{n+1} and ν_{kl}^{n+1} with $\bar{c}_{kl}^m$ and $\bar{\nu}_{kl}^m$ if $k \le i$ and $l \le j$, otherwise with c_{kl}^m and ν_{kl}^m, i.e.,

$$\frac{\bar{c}_{ij}^m}{\Delta t}+\frac{4\bar{\nu}_{ij}^m}{h^2} = \phi_{ij}^n+\frac{\nu_{i+1,j}^m+\bar{\nu}_{i-1,j}^m+\nu_{i,j+1}^m+\bar{\nu}_{i,j-1}^m}{h^2}, \tag{8}$$

$$\frac{h^2+2\epsilon_0^2}{(h^2/2)}\bar{c}_{ij}^m-\bar{\nu}_{ij}^m = -\psi_{ij}^n+\frac{c_{i+1,j}^m+\bar{c}_{i-1,j}^m+c_{i,j+1}^m+\bar{c}_{i,j-1}^m}{(h^2/\epsilon_0^2)}. \tag{9}$$

step 2) *Compute the defect* $(\bar{d_1}^m{}_k, \bar{d_2}^m{}_k) = (\phi_k^n, \psi_k^n) - N_k(\bar{c}_k^m, \bar{\nu}_k^m)$.

step 3) *Restrict the defect and* $\{\bar{c}_k^m,\ \bar{\nu}_k^m\}$

$$(\bar{d_1}^m{}_{k-1}, \bar{d_2}^m{}_{k-1}) = I_k^{k-1}(\bar{d_1}^m{}_k, \bar{d_2}^m{}_k),\ (\bar{c}_{k-1}^m, \bar{\nu}_{k-1}^m) = I_k^{k-1}(\bar{c}_k^m, \bar{\nu}_k^m).$$

step 4) *Compute the right-hand side*

$$(\phi_{k-1}^n, \psi_{k-1}^n) = (\bar{d_1}^m{}_{k-1}, \bar{d_2}^m{}_{k-1}) + N_{k-1}(\bar{c}_{k-1}^m, \bar{\nu}_{k-1}^m).$$

step 5) *Compute an approximate solution* $\{\hat{c}_{k-1}^m,\ \hat{\nu}_{k-1}^m\}$ *of the coarse grid equation on* Ω_{k-1}, *i.e.,*

$$N_{k-1}(c_{k-1}^m, \nu_{k-1}^m) = (\phi_{k-1}^n, \psi_{k-1}^n). \tag{10}$$

If $k = 1$, we explicitly invert a 2×2 matrix to obtain the solution. If $k > 1$, we solve (10) by performing a FAS k-grid cycle using $\{\bar{c}_{k-1}^m,\ \bar{\nu}_{k-1}^m\}$ as an initial approximation:

$$\{\hat{c}_{k-1}^m, \hat{\nu}_{k-1}^m\} = \text{FAScycle}(k-1, \bar{c}_{k-1}^m, \bar{\nu}_{k-1}^m, N_{k-1}, \phi_{k-1}^n, \psi_{k-1}^n, \beta).$$

step 6) *Compute the coarse grid correction* (*CGC*).

$$\hat{v}_{1k-1}^m = \hat{c}_{k-1}^m - \bar{c}_{k-1}^m,\ \hat{v}_{2k-1}^m = \hat{\nu}_{k-1}^m - \bar{\nu}_{k-1}^m.$$

step 7) *Interpolate the correction:* $\hat{v}_{1k}^m = I_{k-1}^k \hat{v}_{1k-1}^m,\ \hat{v}_{2k}^m = I_{k-1}^k \hat{v}_{2k-1}^m$.

step 8) *Compute the corrected approximation on* Ω_k

$$c_k^{m,\text{ after } CGC} = \bar{c}_k^m + \hat{v_1}_k^m,\ \nu_k^{m,\text{ after } CGC} = \bar{\nu}_k^m + \hat{v_2}_k^m.$$

step 9) *Do postsmoothing*

$$\{c_k^{m+1}, \nu_k^{m+1}\} = SMOOTH^\beta(c_k^{m,\text{ after } CGC}, \nu_k^{m,\text{ after } CGC}, N_k, \phi_k^n, \psi_k^n).$$

This completes the description of a nonlinear FAScycle.

4. Numerical simulations

In this section, we first present two- and three-dimensional calculations to verify quantitatively the proposed numerical solution for the phase field model for the anisotropic particle-matrix interfacial energy. We will assume periodic boundary conditions.

4.1. Two-dimensional simulations

The first example is equilibrium shapes of particles in a matrix with two different anisotropic coefficients. This test problem is based on the similar one in Eggleston, McFadden, and Voorhees [3]. The second one is the evolution of a random distribution of concentration.

4.1.1. *Comparison between analytical and phase-field numerical results for equilibrium shapes of particles in a matrix.* Equilibrium shapes are achieved when the chemical potential is constant throughout the system and can be found in parametric form [1]:

$$x = A(\epsilon\cos\theta - \epsilon_\theta\sin\theta),\ y = A(\epsilon\sin\theta + \epsilon_\theta\cos\theta), \tag{11}$$

where A is a constant, $\tan(\theta) = c_y/c_x$, and $\epsilon = \epsilon_0(1 + \epsilon_4\cos(4\theta))$, which is valid for a crystal with four fold symmetry. Missing orientations occur when the reciprocal ϵ - plot first becomes concave [5]. The curvature of a polar plot $r = f(\theta)$ is

$$k = (r^2 + 2r_\theta^2 - rr_{\theta\theta})/(r^2 + r_\theta^2)^{\frac{3}{2}}. \tag{12}$$

For $r = f(\theta) = 1/\epsilon$, Eq. (12) becomes

$$k = (\epsilon + \epsilon_{\theta\theta})/[1 + (\epsilon_\theta/\epsilon)^2]^{\frac{3}{2}}. \tag{13}$$

Since the denominator in Eq. (13) is positive, convexity is lost whenever

$$\epsilon + \epsilon_{\theta\theta} = \epsilon_0(1 - 15\epsilon_4\cos(4\theta)) < 0.$$

Thus, missing orientations occur for $\epsilon_4 > \frac{1}{15}$. The shapes obtained from Eq. (11) include metastable and unstable orientations on the "ears" that do not belong to the equilibrium crystal. Mullins [10] proved that in two dimensions the equilibrium shape is given by the convex shape remaining after removal of these "ears". We test the numerical stability by employing an initial particle that has all orientations, a circle, with $\epsilon_4 = 0.05$ and $\epsilon_4 = 0.2$. The evolution shapes were computed using the circular shape as the initial condition, i.e.,

$$c(x,y) = \tanh\left(\frac{0.25 - \sqrt{(x-0.5)^2 + (y-0.5)^2}}{\sqrt{2}\epsilon_0}\right),$$

where $\epsilon_0 = 0.0113$. We take the spatial domain to be $\Omega = [0,1] \times [0,1]$, the mesh size to be 128×128, and time step to be $\Delta t = 100h$. This time step is vary large compared to other methods. For example, a very small time step, $\Delta t = 10^{-9}$, was necessary to adequately resolve the motion [11].

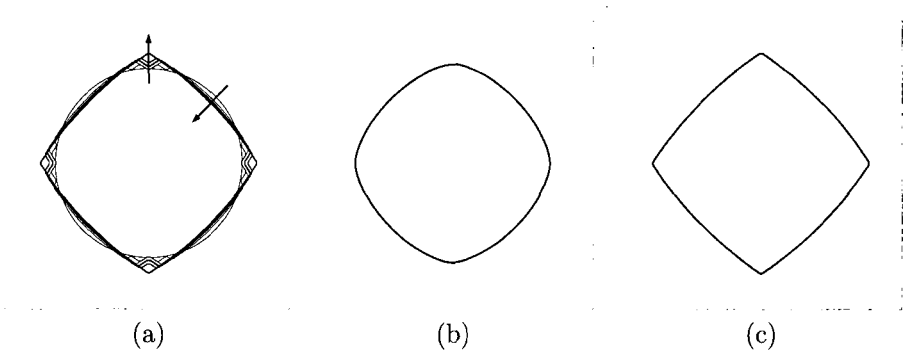

FIGURE 1. (a) Surface contours during computation of an equilibrium shape for $\epsilon_4 = 0.2$. The arrows denote the direction of motion of the interface. Comparison of numerical *solid line* and exact *dotted line* for the various values of ϵ_4: (b) $\epsilon_4 = 0.05$ and (c) $\epsilon_4 = 0.2$.

The evolution with $\epsilon_4 = 0.2$ is shown in Fig. 1(a) by contours of $c = 0$ at various times. The arrows denote the direction of motion of the interface. Even though the initial condition contains missing orientations, the calculations get rid of missing orientations quickly and evolve to the equilibrium state, validating the stability of the method.

Let us consider the influence of the strength of the anisotropic coefficient, ϵ_4. Fig. 1(b) and (c) show this agreement in both the numerical (solid line) and the exact (dotted line) equilibrium shapes for $\epsilon_4 = 0.05$ and 0.2, respectively. In the case of $\epsilon_4 = 0.05$, both numerical and exact results are almost identical and one overlaps the other. In the case of $\epsilon_4 = 0.2$, the situation is same except the ears that do not belong to the equilibrium shape.

4.1.2. *Evolution of a random distribution.* To illustrate the robustness of the proposed method, we examine the evolution of a random distribution of concentration. We take the same parameters in the previous calculation except the initial condition and a smaller time step for the time accurate calculation. The initial state is $c(x, y) = -0.3 + rand(x, y)$, where $rand(x, y)$ is a random number between -0.01 and 0.01.

The phase-field model easily handles complicated interfacial geometries without difficulties. In Fig. 2, the evolution of interfaces from random initial configuration with $\epsilon_4 = 0.05$ (top) and $\epsilon_4 = 0.2$ (bottom) is shown. The result demonstrates that the method can simulate numerically cases of multiple particles surrounded by a matrix phase. It also handles naturally topological change such as interface merging as shown in top figures. At early stages, islands self organize into a relative uniform and regular array, and then ripening occurs. At later stages, the particles resemble equilibrium shapes. We next consider three-dimensional calculations.

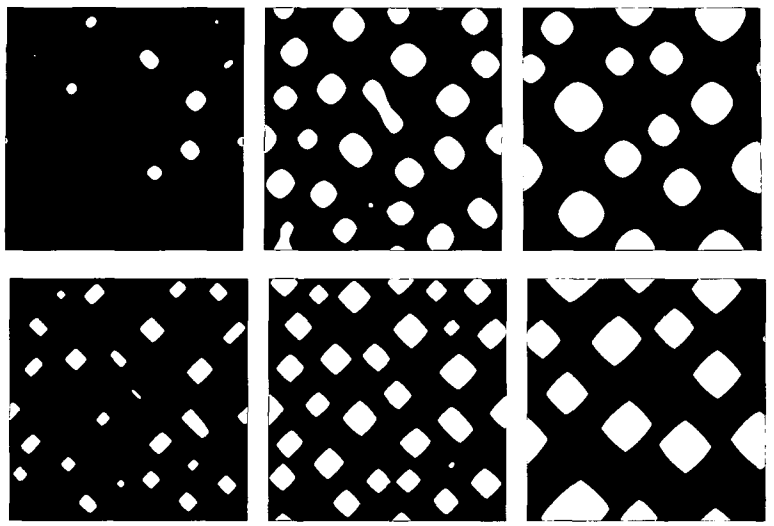

FIGURE 2. Evolution of interface from random with $\epsilon_4 = 0.05$ (top) and $\epsilon_4 = 0.2$ (bottom). The times are t=0.15, 0.45, and 5.90.

4.2. Three-dimensional simulations

In addition to the two-dimensional calculations previously described, a series of three-dimensional calculations are performed in order to further evaluate the present numerical solution for the phase field model.

4.2.1. *Equilibrium shapes of particles in a matrix.* Hoffman and Cahn [6] developed the $\boldsymbol{\xi}$-vector to describe surface energy anisotropy in a first-order phase transition represented by a sharp interface. In the three-dimensional space, by employing spherical coordinates, the equilibrium shape can be described by the $\boldsymbol{\xi}$-vector and is given by

$$\boldsymbol{\xi} = \epsilon(\mathbf{n})\hat{\mathbf{n}} + \epsilon_\theta(\mathbf{n})\hat{\boldsymbol{\theta}} + \frac{\epsilon_\varphi(\mathbf{n})}{\sin\theta}\hat{\boldsymbol{\varphi}},$$

where $\hat{\mathbf{n}} = (\sin\theta\cos\varphi,\ \sin\theta\sin\varphi,\ \cos\theta)$, $\hat{\boldsymbol{\theta}} = (\cos\theta\cos\varphi,\ \cos\theta\sin\varphi,\ -\sin\theta)$, and $\hat{\boldsymbol{\varphi}} = (-\sin\theta\sin\varphi, \sin\theta\cos\varphi, 0)$ are unit vectors of the spherical coordinate system. Fig. 3 shows $\boldsymbol{\xi}$-plots for

$$\begin{aligned}\epsilon(\mathbf{n}) &= \epsilon_0(1-3\epsilon_4)\left[1+\frac{4\epsilon_4}{1-3\epsilon_4}\frac{c_x^4+c_y^4+c_z^4}{|\nabla c|^4}\right] \\ &= \epsilon_0(1-3\epsilon_4)\left[1+\frac{4\epsilon_4}{1-3\epsilon_4}\left(\sin^4\theta(\cos^4\varphi+\sin^4\varphi)+\cos^4\theta\right)\right]\end{aligned}$$

with (a) $\epsilon_4 = 0.05$ and (b) $\epsilon_4 = 0.2$. See the Appendix for the Mathematica software code for the graph generation. For $\epsilon_4 = 0.05$, all orientations appear

on the equilibrium shape. For $\epsilon_4 = 0.2$, the $\boldsymbol{\xi}$ plot has ears and flaps that must be truncated to give the equilibrium shape, which resembles an octahedron with curved faces. For more details about $\boldsymbol{\xi}$-vector for equilibrium shape, the reader is referred to [16].

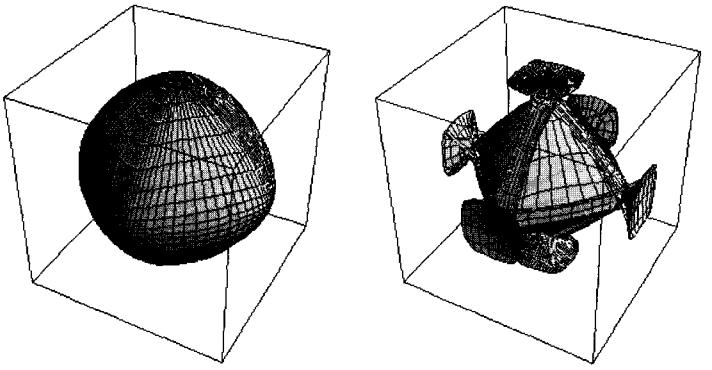

(a) (b)

FIGURE 3. $\boldsymbol{\xi}$-plots for $\epsilon(\mathbf{n}) = \epsilon_0(1 - 3\epsilon_4)[1 + 4\epsilon_4(c_x^4 + c_y^4 + c_z^4)/((1 - 3\epsilon_4)|\nabla c|^4)]$ with (a) $\epsilon_4 = 0.05$ and (b) $\epsilon_4 = 0.2$.

We test the numerical stability by employing an initial particle that has all orientations, a circle, with $\epsilon_4 = 0.05$ and $\epsilon_4 = 0.2$. The evolution shapes were computed using the sphere shape as the initial condition, i.e.,

$$c(x, y, z) = \tanh\left(\frac{0.25 - \sqrt{(x - 0.5)^2 + (y - 0.5)^2 + (z - 0.5)^2}}{\sqrt{2}\epsilon_0}\right),$$

where $\epsilon_0 = 0.02$. The mesh size is $128 \times 128 \times 128$, domain size is $\Omega = [0, 1] \times [0, 1] \times [0, 1]$, and time step is $\Delta t = 100h$. Even though the initial condition is unlikely to occur in nature because it contains missing orientations, the calculation illustrates that the method is stable. Fig. 4 shows the evolution of interface from a sphere with radius, 0.25. The top and the bottom rows are with $\epsilon_4 = 0.05$ and $\epsilon_4 = 0.2$, respectively. We found the equilibrium shapes are in good agreements with the exact ones.

4.2.2. *Evolution of a random distribution.* Fig. 5 shows evolution of interface from a random initial condition with average concentration $c = -0.3$, $\epsilon_0 = 0.0113$, and $\epsilon_4 = 0.2$. From Figs. 5(a)-5(c), it is clear that there is a rapid initial transient evolution of the phase field to $c = -1$ or 1. Subsequently, coarsening behavior of the particle phase continues until t = 1.56, which is the final time displayed. Note that the last Fig. 5(c) does not mean the equilibrium state of the process. This result shows the robustness of the proposed numerical solution.

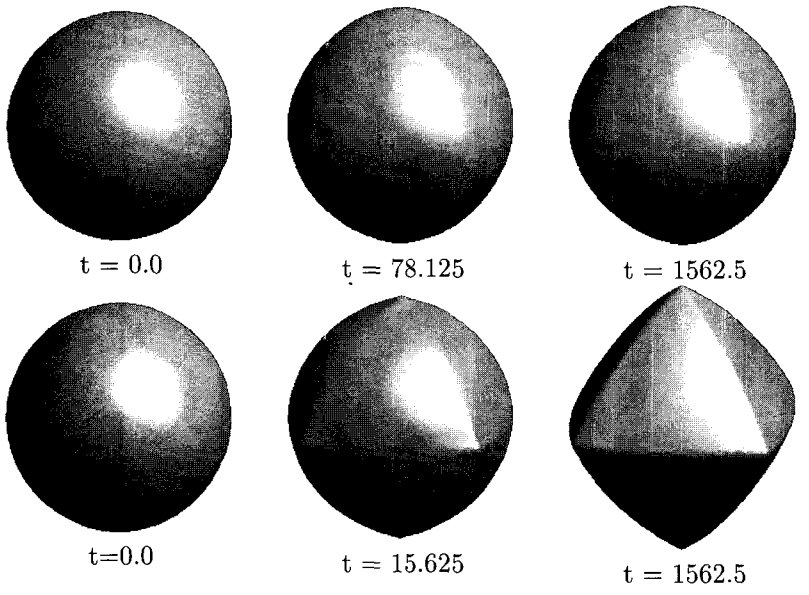

FIGURE 4. Evolution of interface from a sphere with radius, 0.25. The top and the bottom rows are with $\epsilon_4 = 0.05$ and $\epsilon_4 = 0.2$, respectively.

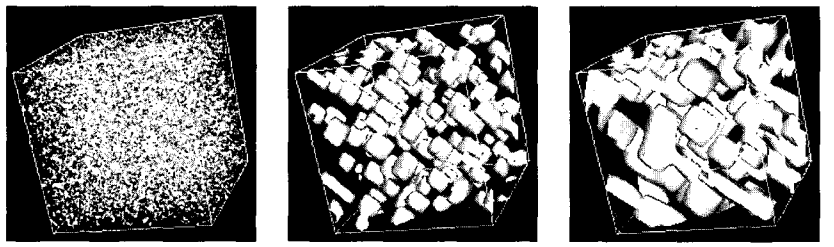

FIGURE 5. Evolution of interface from a random initial condition with average concentration $c = -0.3$, $\epsilon_0 = 0.0113$, and $\epsilon_4 = 0.2$.

5. Conclusion

An efficient and accurate numerical scheme and its nonlinear multigrid solver for the phase-field model for systems with anisotropic interfacial energy have been developed. The computed equilibrium particle shapes, both with and without sharp corners, are in excellent agreement with the exact results. The most important feature of the proposed scheme is that the method employs an

unconditionally stable scheme that allows a large time step. The large time step is very important in studying three-dimensional simulations.

Acknowledgment. This work was supported by the Korea Research Foundation Grant funded by the Korean Government(MOEHRD)(KRF-2006-C00225).

Appendix A. Mathematica Code for Fig. 3(b)

```
<< Graphics'ParametricPlot3D'
e0 = 0.0113;  e4 = 0.2;
e[t_,p_]:=e0(1 - 3e4)(1 + (4e4/(1 - 3e4))
            (Sin[t]^4(Cos[p]^4+Sin[p]^4)+Cos[t]^4);
x=e[t,p]Sin[t]Cos[p]+D[e[t,p],t]Cos[p]Cos[t]-
      Sin[p]D[e[t,p],p]/Sin[t];
y=e[t,p]Sin[t]Sin[p]+D[e[t,p],t]Sin[p]Cos[t]+
      Cos[p]D[e[t,p],p]/Sin[t];
z=e[t,p]Cos[t]-D[e[t,p],t]Sin[t];
ParametricPlot3D[{x,y,z},{t,0,2Pi},{p,0,Pi},
PlotPoints->40,Axes -> False];
```

References

[1] W. K. Burton, N. Cabrera, and F. C. Frank, *The growth of crystals and the equilibrium structure of their surfaces*, Trans. R. Soc. Lond. A **243** (1951), 299–358.

[2] J. W. Cahn and J. E. Hilliard, *Free energy of a nonuniform system. I. Interfacial free energy*, J. Chem. Phys. **28** (1958), 258–267.

[3] J. J. Eggleston, G. B. McFadden, and P. W. Voorhees, *A phase-field model for highly anisotropic interfacial energy*, Physica D **150** (2001), 91–103.

[4] D. J. Eyre, *An unconditionally stable one-step scheme for gradient systems*, Preprint, University of Utah, Salt Lake City, 1997.

[5] F. C. Frank, *Metal Surfaces*, ASM, Cleveland, OH, 1963.

[6] D. W. Hoffman and J. W. Cahn, *A vector thermodynamics for anisotropic surfaces. I. Fundamentals and application to plane surface junctions*, Surf. Sci. **31** (1972), 368–388.

[7] J. S. Kim, *A continuous surface tension force formulation for diffuse-interface models*, J. Comput. Phys. **204** (2005), 784–804.

[8] J. S. Kim and J. Sur, *A hybrid method for higher-order nonlinear diffusion equations*, Commun. Korean Math. Soc. **20** (2005), no. 1, 179–193.

[9] B. P. Vollmayr-Lee and A. D. Rutenberg, *Fast and accurate coarsening simulation with an unconditionally stable time step*, Phys Rev E, **68** (2003), 1–13.

[10] W. W. Mullins, *Proof that the two dimensional shape of minimum surface free energy is convex*, J. Math. Phys. **3** (1962), 754–759.

[11] M. Siegel, M. J. Miksis, and P. W. Voorhees, *Evolution of material voids for highly anisotropic surface energy*, J. Mech. Phys. Solids **52** (2004), 1319–1353.

[12] T. Takaki, T. Hasebe, and Y. Tomita, *Two-dimensional phase-field simulation of self-assembled quantum dot formation*, J. Crystal Growth **287** (2006), 495–499.

[13] U. Trottenberg, C. Oosterlee, and A. Schüller, *MULTIGRID*, Academic Press, 2001.

[14] A. A. Wheeler, W. J. Boettinger, and G. B. McFadden, *Phase-field model for isothermal phase transitions in binary alloys*, Phys. Rev. A **45** (1992), 7424–7439.

[15] Y. Wang, L. Q. Chen, and A. G. Khachaturyan, *Kinetics of strain-induced morphological transformation in cubic alloys with a miscibility gap*, Acta Metall. **41** (1993), 279–296.

[16] A. A. Wheeler and G. B. McFadden, *On the notion of a $\boldsymbol{\xi}$-vector and a stress tensor for a general class of anisotropic diffuse interface models*, Proc. R. Soc. Lond. A **453** (1997), 1611–1630.

[17] Y. W. Zhang, *Self-organization, shape transition, and stability of epitaxially strained islands*, Phys. Rev. B **61** (2000), 388–392.

Department of Mathematics
Dongguk University
Seoul 100-715, Korea
E-mail address: cfdkim@dongguk.edu
URL: http://math.uci.edu/~jskim/